IEEE Access
Multidisciplinary | Rapid Review | Open Access Journal

Received October 23, 2021, accepted November 1, 2021, date of publication November 4, 2021, date of current version November 12, 2021.

Digital Object Identifier 10.1109/ACCESS.2021.3125317

Design of Cascaded PI-Fractional Order PID Controller for Improving the Frequency Response of Hybrid Microgrid System Using Gorilla Troops Optimizer

MOETASEM ALI, HOSSAM KOTB, KAREEM M. ABORAS, AND NABIL H. ABBASY, (Senior Member, IEEE)

Department of Electrical Engineering, Faculty of Engineering, Alexandria University (AU), Alexandria 21544, Egypt

Corresponding author: Hossam Kotb (hossam.kotb@alexu.edu.eg)

ABSTRACT This paper proposes a cascaded Proportional Integral-Fractional Order Proportional-Integral-Derivative (PI-FOPID) controller to improve the frequency response of a hybrid microgrid system. The optimum gains of the proposed controller are fine-tuned using Gorilla Troops Optimizer (GTO) which is a recent metaheuristic optimization algorithm. The case study is a two-area microgrid system that contains diesel generators, various renewable energy sources such as photovoltaic and wind generation systems, as well as different energy storage devices. Moreover, real wind speed and solar irradiance measurements have been collected for proper system modeling. The performance of the proposed cascaded PI-FOPID controller is compared to the single structure fractional order PID (FOPID) controller based on GTO and numerous other optimization techniques presented in the previous literature such as Genetic Algorithm and Particle Swarm Optimization. The robustness of the proposed cascaded PI-FOPID controller is investigated under different scenarios such as different step load perturbations, random load disturbances, and renewable energy sources variation. The simulation results are carried out using MATLAB/Simulink. The results show that the proposed controller provides an improvement in the maximum overshoot/undershoot and settling time of 99.8% and 75.9%, respectively, compared to other competing techniques.

INDEX TERMS Cascaded PI- fractional order proportional-integral-derivative controller, gorilla troops optimizer, hybrid microgrid system, load frequency control, renewable sources, two-area system.

NOMENCLATURE

ACE	Area control error.
A_{rs}	Rotor swept area.
B_1, B_2	Frequency bias coefficients.
BES	Battery energy storage.
$C_1(s)$, $C_2(s)$	Controller transfer functions.
C_p	Power coefficient of wind turbine.
D, F, J, O, S, V, N	Calculated variables in GTO algorithm.
DEG	Diesel engine generator.
FF	Fitness function.
FOPID	Fractional order proportional-integral-derivative.
GA	Genetic algorithm.
GTO	Gorilla troops optimizer.
GX(i)	Position vector of a candidate gorilla.
$GX_r(t)$	Random gorilla member position.
GX(t+1)	Position of candidate gorilla in the next iteration.
IAE	Integral absolute error.
ITAE	Integral time absolute error.
K_A	Area swing coefficient.
K_B	Battery energy storage gain.
K_{CV}	Gain of control valve model.
K_{DE}	Gain of DEG model.
K_{PV}	Gain of PV model.
K_{SM}	Gain of superconducting magnetic energy storage model.
K_W	Gain of wind turbine generator model.

The associate editor coordinating the review of this manuscript and approving it for publication was Nagesh Prabhu.

This work is licensed under a Creative Commons Attribution 4.0 License. For more information, see https://creativecommons.org/licenses/by/4.0/

K_{d2}	Derivative gain of FOPID controller.
K_{i1}	Integral gain of PI controller.
K_{i2}	Integral gain of FOPID controller.
K_{p1}	Proportional gain of PI controller.
K_{p2}	Proportional gain of FOPID controller.
K_{tie}	Synchronizing Coefficient.
LFC	Load frequency control.
L_r	Lower boundary of variables.
MO	Maximum overshoot.
MU	Maximum undershoot.
MaxIt	Maximum number of iterations.
PI	Proportional-integral.
PID	Proportional-integral-derivative.
PSO	Particle swarm optimization.
PV	Photovoltaic.
P_{BES}	Output power of BES model.
P_{DEG}	Output power of DEG model.
P_{PV}	Output power of PV model.
$P_{PV,STC}$	Rated PV output power under standard test conditions.
P_{SM}	Output power of superconducting magnetic energy storage model.
P_W	Input power of wind turbine generator model.
P_{WT}	Output power of wind turbine generator model.
R	Impact force.
R_1, R_2	Droops.
RES	Renewable energy source.
r_1, r_2, r_3, *rand*	Random variables in the optimization algorithm.
SLP	Step load perturbation.
SMES	Superconducting magnetic energy storage.
S_W	Wind turbine speed.
T	Coefficient vector to estimate the violence level.
T_a	Ambient temperature.
T_r	Reference temperature.
T_s	Settling time.
t	Number of iterations.
t_s	Simulation time.
U_C	Output signal of PI-FOPID controller.
U_r	Upper boundary of variables.
WTG	Wind turbine generator.
$X(t)$	Current gorilla position vector.
$X_r(t)$	Random gorilla member.
$X_{silverback}$	Position vector of silverback.
τ_A	Area swing time constant.
τ_B	Time constant of BES model.
τ_{SM}	Time constant of SMES model.
τ_{CV}	Time constant of control valve model.
τ_{DE}	Time constant of DEG model.
τ_{PV}	Time constant of PV model.
τ_W	Time constant of WTG model.
μ	Derivative order.
ΔF_1	Frequency deviation in area 1.
ΔF_2	Frequency deviation in area 2.
ΔP_{tie}	Tie-line power deviation.
α	Temperature coefficient.
η_{MPPT}	Maximum power point tracking efficiency.
λ	Integral order.
ρ	Air density.
$\emptyset_S$	Solar irradiance.
$\emptyset_{STC}$	Solar irradiance under standard test conditions.

I. INTRODUCTION

A hybrid microgrid system is a combination of several parallel distributed resources connected with electronically-controlled strategies, which are capable of operating in both island and grid-connected mode [1], [2]. Renewable energy sources (RES) provide clean and safe energy while reducing carbon dioxide emissions as well as global warming phenomenon, yet they are constrained by weather changes [3], [4]. The high penetration of renewable energy sources increases the difficulty of microgrid control, as traditional controllers cannot deal with the fluctuations and uncertainties of renewable energy sources [5]. Moreover, the variation of RES and sudden load disturbances may cause severe problems such as power sharing deterioration causing system frequency to deviate from its limits [6]. As a result, an effective load frequency control (LFC) is necessary to keep the frequency deviations within acceptable limits particularly when the grid is working in a standalone mode [7].

Numerous control approaches have been presented in previous literature to enhance the performance of the LFC design. Classical PID controllers have been commonly used in the load frequency control model due to their simple design. Moreover, different optimization algorithms have been suggested to tune the PID controller parameters such as whale optimization algorithm [8], improved genetic algorithm [9], particle swarm optimization [10], [11], lightning attachment procedure optimization [11], marine predators algorithm [12], social spider optimizer [13], and cuckoo search algorithm [14]. Furthermore, the PID controller has been suggested to be used as a load frequency controller for three unequal hybrid microgrids with solar, wind and energy storage systems in [15] and tuned by Quasi-oppositional chaotic Selfish-herd optimization algorithm. In addition, researchers have suggested that the PID controller can be modified by combining it with a linear quadratic gaussian approach as in [16], [17], where the robustness of this combination is high and can be used for frequency stabilization in the hybrid microgrid systems. Non-classical controllers have been applied as well [18]–[20]. The load frequency control can be implemented using frequency division and sliding mode algorithm where the controller design is based on the division of error into high and low frequency components as presented in [18]. In addition, model predictive control can be used to improve the load frequency control performance in multi-area systems as presented in [19], [20].

Recently, researchers have introduced several modifications to the PID controller due to its low ability to control severe disturbances such as sudden load perturbations and RES fluctuations. Some researchers suggested that PID controller could be combined with the fuzzy logic controller to further enhance the system frequency stability as presented in [21], [22]. A fractional order PID (FOPID) controller has been suggested in [23] for the load frequency control design based on the fractional order calculus. The main advantage of FOPID controller is that it gives n degrees of freedom as to improve the controller efficiency, flexibility, and robustness [24]. In [25], a synthesis between the moth flame optimization algorithm and the generalized Hopfield neural network has been suggested for tuning the both the FOPID controller gains and the integrator and derivative orders. The robustness of FOPID controller was then tested in [26] when electric vehicles were introduced into the microgrid system, and their parameters were tuned using a slap swarm algorithm. In addition, the performance of FOPID controller for automatic generation control in multi-area systems has been improved using genetic algorithm (GA) [27], particle swarm optimization (PSO) [28], and grasshopper optimization algorithm [29]. Moreover, the FOPID of an automatic voltage regulator system using multi-objective chaotic optimization has been used in [30], where the frequency domain has been used to test the stability and robustness of the controller. In [31], a combination of FOPID and Tilt-integral derivative controllers for LFC as well as SMES model output has been proposed, in which the controller parameters have been tuned by the manta ray forage optimization algorithm. In addition, the yellow saddle goat algorithm has been used to tune PIFOD-(1 + PI) in [32] to maintain the frequency stability in the two-area hybrid microgrid system. A non-linear FOPID controller has been proposed in [33] to control the frequency of Egyptian power grid integrated with PV and wind energy sources where it combines the advantages of non-linear PID and FOPID controllers.

Nowadays, the cascaded controller configuration provides better system performance compared to the single controller structure. For example, a cascaded FOPI-FOPD controller based on dragonfly search algorithm has been suggested in [34] for advanced LFC of power systems. In [35], the combination of FOPID and Tilt-integral derivative controllers provided better frequency regulation in the power system. In a parallel track, Artificial Gorilla Troops optimizer (GTO) has recently been published as a metaheuristic optimization algorithm based on the nature life of gorillas [36]. The GTO optimizer showed high accuracy and efficiency in optimizing various engineering problems such as in [37]. In addition, the GTO algorithm has an excellent ability to achieve good results and acceptable performance for different system dimensions by increasing the level of search capabilities. It also has a significant advantage over other optimizers in all comparable dimensions because other optimizers significantly reduce their performance as the dimensions increase. Another advantage of the GTO is that it has an excellent ability to balance exploration and exploitation capabilities in the face of large-scale issues [36]. In contrast, the GA has some limitations such as the fitness value getting evaluated on a set of generations, and this can be an expensive process for a certain number of problems. If a Genetic algorithm is not used in the best manner, it may not converge to an optimal solution. However, the disadvantages of the PSO algorithm are that it is easy to fall into local optimum in high-dimensional space and has a low convergence rate in the iterative process.

In order to further improve the frequency control of a hybrid two-area microgrid system, a new cascaded PI-FOPID controller design is proposed in this paper. The parameters of the proposed controller in each area are optimized using GTO algorithm, as a novel metaheuristic optimization technique that has not been used before with the load frequency control design. The main contributions of this paper can be summarized as follows:

- Improving the frequency response of a hybrid microgrid system using a robust cascaded PI-FOPID controller.
- Optimizing the parameters of the proposed PI-FOPID controller using GTO algorithm which is a new effective optimization technique that has not been applied before for load frequency control design.
- Using real data of wind speed and solar irradiance measurements for proper system modelling.
- Testing the effectiveness of the proposed controller when the microgrid system subjected to various disturbances such as different step load perturbations, random load variation and RES fluctuation.

The rest of the paper is organized as follows: Section 2 presents the architecture of the hybrid microgrid system where each component is briefly explained. The proposed GTO algorithm is introduced in Section 3, while Section 4 presents the proposed controller structure and problem formulation. Section 5 shows the results of different scenarios and their discussion. Finally, Section 6 concludes the paper.

II. HYBRID MICROGRID SYSTEM ARCHITECTURE

The microgrid case study system is shown in Figure 1 which consists of two areas connected by a tie-line to improve the reliability of supply in each area. Area 1 contains different energy sources such as a wind turbine, a valve-controlled diesel generator, in addition to a superconducting magnetic energy storage (SMES) and a step load. Area 2 contains a PV energy source, a battery energy storage (BES), another valve-controlled diesel generator, and a step load as shown in Figure 1. For our microgrid case study, the wind turbine system is assumed to supply about 20% of the total microgrid load and the PV system is assumed to supply about 25% of the total demand. Both diesel generators supply about

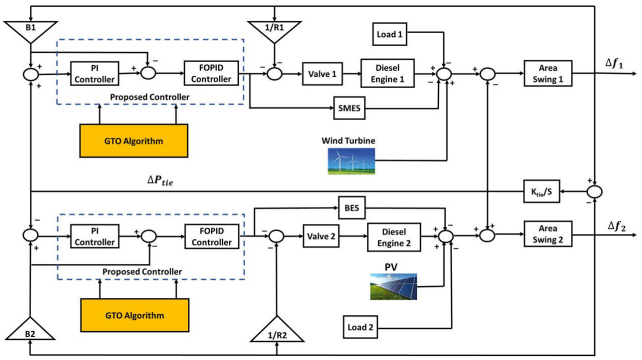

FIGURE 1. Block diagram representation of the two-area hybrid microgrid system [2].

55% of the total demand. Moreover, the energy storage in each area is considered to have the same capacity as the renewable energy connected to it. When the microgrid system is subjected to sudden load disturbances and/or RES fluctuations such as solar radiation change and wind speed variation, this may cause the system unstable. Therefore, each area is controlled by a proposed cascaded PI-FOPID controller that is tuned by the GTO algorithm to minimize the frequency deviation in each area (ΔF_1, ΔF_2) and the tie-line power deviation (ΔP_{tie}). Moreover, the performance of the GTO-based cascaded PI-FOPID controller is compared to the single FOPID controller based on GA, PSO, and GTO algorithms. For simplicity, each component in the microgrid system is assumed to be linear and can be modeled using a first-order transfer function via Matlab/Simulink. This assumption has been effectively used for system modeling in previous literature, as in [2] and [38]. Furthermore, transfer function models and typical values for the various components of the case study system are briefly discussed in the following subsections:

A. WIND TURBINE GENERATING (WTG) MODEL

The power generated by the aerodynamics of wind turbine (P_W) can be calculated as follows [39]:

$$P_W = 0.5 \times A_{rs} \times \rho \times C_p \times S_w^3 \tag{1}$$

where A_{rs} is the swept area of the rotor, ρ is the air density, C_p is the power coefficient, and S_w represents the wind speed. The power coefficient C_p is generally controlled to allow optimum power for wind turbines. In this study, the wind turbine generating system can be modeled using a first-order transfer function for small-signal stability of the system as shown in Figure 2. The linear WTG model has a gain K_w of 1 and a time constant τ_w of 1.5 seconds [2].

Moreover, real wind speed data have been collected for this study from a typical wind turbine farm near Zafarana, Egypt (latitude of 29.23° N and longitude of 32.59° E) in April 2020. The average wind speed in the site ranges between 6 and 14 m/sec as shown in Figure 3 [2] and the

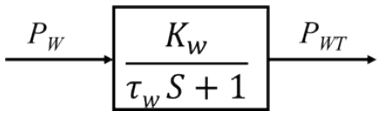

FIGURE 2. Block diagram of WTG model.

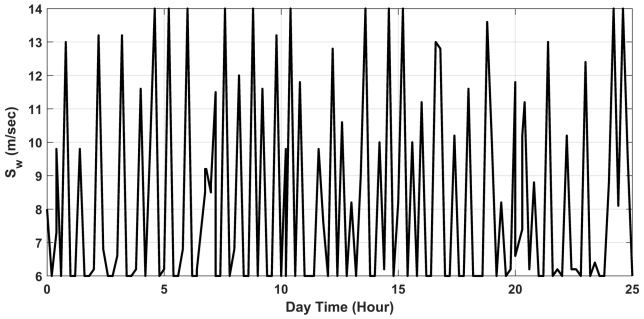

FIGURE 3. Daily variation of wind speed [2].

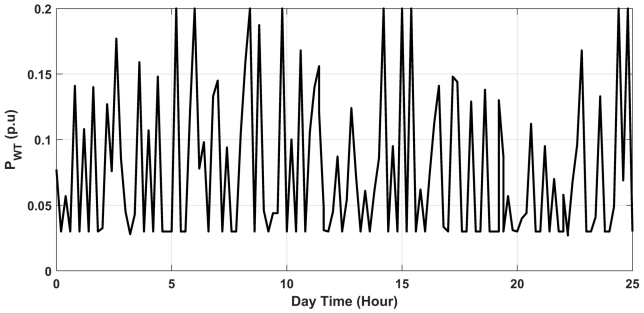

FIGURE 4. Daily variation of WTG model output power.

output power variation of WTG model fluctuates between 0.03 and 0.2 p.u during the day as shown in Figure 4.

B. PHOTOVOLTAIC (PV) MODEL

The PV module output power (P_{PV}) is mainly determined by the ambient temperature (T_a) and solar irradiance ($\emptyset_s$) on the PV array's surface. The calculation of PV output power (P_{PV}) can be represented as follows [2], [38]:

$$P_{PV} = P_{PV,STC} \times (\emptyset_s/\emptyset_{STC}) \times (1 + \alpha\,(T_a - T_r)) \times \eta_{MPPT} \tag{2}$$

where $P_{PV,STC}$ is the rated output power under standard test conditions (STC), $\emptyset_{STC}$ indicates the solar irradiance under STC with a typical value of 1000 W/m^2, α indicates the temperature coefficient, T_r is the reference temperature with a typical value of 25°C, and η_{MPPT} represents the efficiency of maximum power point tracking. In this study, the PV system is simply modeled using a first-order transfer function as the PV power varies linearly with the solar radiation as shown in Figure 4. The PV model has a gain K_{PV} of 1 and a time constant τ_{PV} of 0.03 seconds [2].

Moreover, the input solar radiation fed to the PV model is collected from a real PV station of a capacity 1.5 GW

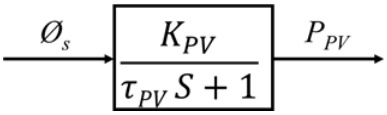

FIGURE 5. Block diagram of PV model [40].

located in Aswan, Egypt (latitude of 24.08° N and longitude of 32.89° E) in July 2020. The solar irradiance in the site has a normal distribution shape with a maximum of 1000 W/m^2 as shown in Figure 6 [41]. Furthermore, Figure 7 shows the variation of PV output power with a maximum of 0.25 p.u.

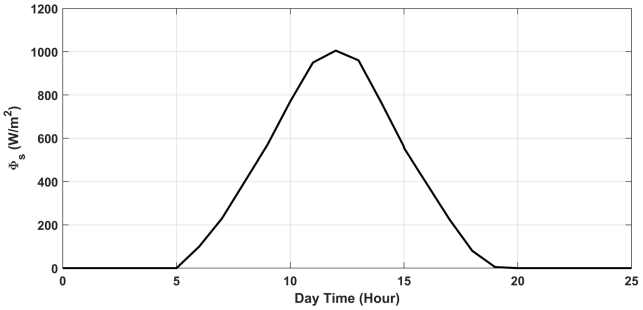

FIGURE 6. Daily variation of solar irradiance [41].

C. DIESEL ENGINE GENERATOR (DEG) MODEL

Generally, DEGs are integrated with renewable energy resources to supply backup power for standalone microgrid systems due to the intermittent nature of RES [42]. A control valve is installed with the diesel power generating system to control the output power of the diesel engine [43]. The DEG model can be simply represented by a first-order transfer function as shown in Figure 8. The valve gain K_{CV} and time constant τ_{CV} are 1 and 0.05 seconds, respectively. In addition, the linear model of the diesel generator has a gain K_{DE} of 1 and a time constant τ_{DE} of 0.5 seconds [2].

D. SUPERCONDUCTING MAGNETIC ENERGY STORAGE (SMES) MODEL

SMES is a new technology for storing energy from the grid by using a superconducting coil with a negligible magnetic energy loss. Moreover, the main advantages of the SMES devices are their high efficiency, long lifetime and fast response [44]. In this study, the SMES model can be linearized by a first-order transfer function as shown in Figure 9. The SMES model has a time constant τ_{SM} of 0.03 seconds and a gain K_{SM} of 0.98 [2].

E. BATTERY ENERGY STORAGE (BES) MODEL

In this study, the BES can be linearized by a first-order transfer function as shown in Figure 10. The BES has a gain K_B of 1.8 and a time constant τ_B 0.001 seconds [2].

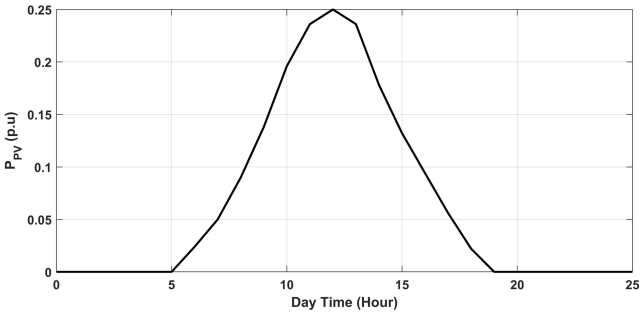

FIGURE 7. Variation of PV model output power.

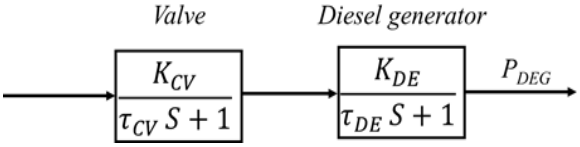

FIGURE 8. Block diagram of DEG model.

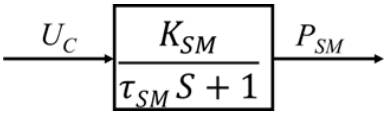

FIGURE 9. Block diagram of SMES model.

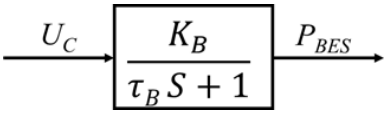

FIGURE 10. Block diagram of BES model.

TABLE 1. Design values of system model parameters [38].

Model	Transfer function	Design parameters
Area swing	$\frac{K_A}{\tau_A S+1}$	$K_{A1}=K_{A2}=1$ $\tau_{A1}=\tau_{A2}=3$
Synchronizing coefficient	$\frac{K_{tie}}{S}$	$K_{tie}=1.4\pi$
Frequency bias coefficients	B_1, B_2	$B_1 = B_2 = 21$
Droops	R_1, R_2	$R_1 = R_2 = 0.05$

Furthermore, the transfer functions and design parameters of the area swing, synchronizing coefficient, frequency bias coefficients and droops can be summarized as shown in Table 1. The proposed optimization algorithm will be presented in the next section.

III. GORILLA TROOPS OPTIMIZATION ALGORITHM (GTO)

GTO is a novel metaheuristic algorithm based on the social intelligence of gorilla troops in nature. The propensity of

$$GX(t+1) = \begin{cases} (U_r - L_r)\, r_1 + L_r, & if\ rand < O \\ (r_2 - D)\, X_r(t) + S \times V, & if\ rand \geq 0.5 \\ X(i) - S(S(X(t) - GX_r(t)) + r_3(X(t) - GX_r(t))), & if\ rand < 0.5 \end{cases} \quad (3)$$

gorillas to live in groups prohibits them from living alone. As a result, they hunt for food as a group and continue to live under the leadership of a silverback gorilla who determines all choices of the group. In this algorithm, the silverback is considered as the best solution, then the gorilla's candidates tend to approach to it and leave the weakest member as it is the worst solution. Moreover, this algorithm is based on two phases as follows [36], [37]:

A. EXPLORATION PHASE

In this phase, each gorilla is configured as a candidate to the best solution in each iteration and the best solution is called the silverback gorilla. Furthermore, there are three different mechanisms that can be summarized in Equation (3) [36], [37], as shown at the top of the page, where O represents the migration to an unknown location parameter, *rand* is a random variable, $X(t)$ indicates the current vector of gorilla position, $X(i)$ indicates the candidate gorilla member number, and $GX(t+1)$ represents the vector of candidate gorilla position in the next iteration. Moreover, L_r and U_r represent the lower and upper limits of the problem variables, respectively. $X_r(t)$ represents one of the gorilla candidates that is selected randomly and $GX_r(t)$ indicates the position of this random gorilla. Further, r_1, r_2 and r_3 are random variables with a range of [0, 1]. The parameter D can be calculated as follows [36], [37]:

$$D = N \times (1 - t/MaxIt) \quad (4)$$

where t and $MaxIt$ are the current iteration and the maximum number of iterations in the optimization problem, respectively.

B. EXPLOITATION PHASE

In this phase, there are two different mechanisms that can be applied. The first mechanism is called "Follow the silverback" and the other one is called "Competition for adult females". Each technique can be selected by comparing the value of D calculated in Equation (4) with a random variable W that is initially selected in the optimization process [36], [37].

1) FOLLOW THE SILVERBACK

The gorillas obey all of Silverback's commands to go to various locations in searching about food supplies and this strategy can be applied when $D \geq W$, hence this behaviour can be represented using Equation (5) [36], [37]:

$$GX(t+1) = S \times J(X(t)X_{silverback}) + X(t) \quad (5)$$

where $X_{silverback}$ represents the position vector of the silverback, S and J are chosen variables.

2) COMPETITION FOR ADULT FEMALES

When juvenile gorillas reach puberty, they compete with other male gorillas to extend their group by selecting adult females, where this process is often a violent conflict. Furthermore, this strategy can be applied when $D < W$, hence Equation (6) can represent this mechanism [36], [37]:

$$GX(i) = X_{silverback}(X_{silverback} \times R - X(t) \times R) \times T \quad (6)$$

where R and T represent the impact force which can be calculated randomly and the coefficient vector to estimate the violence level, respectively. Finally, all solutions of GX(t) are estimated at the end of exploitation phase, then a comparison is made between $X(t)$ and $GX(t)$. If $X(t)$ is larger than the cost of $GX(t)$, then $GX(t)$ will take the value of $X(t)$ and it is called the silverback. Finally, the final values of the algorithm parameters in this work are summarized in Table 2.

TABLE 2. GTO final parameters setting.

GTO Parameter	Value
O	0.03
D	0
S	0
V	0
$rand, r_1, r_2, r_3$	0.85
W	0.8
J	[18.89 28.6 96.84 3.625 0.494 40.6 0.574 71.35 80.1 63.38 41.9 0.566 22.49 0.444]
R	0.7
T	[-0.297 -2.12 1.97 0.132 5.196 0.291 -2.35 1.5 0.429 -0.998 0.228 0.95 3.8 3.12]

Moreover, the steps of the GTO algorithm can be summarized as follows:

1- Initialize all parameters in the algorithm, then evaluate the initial fitness value.
2- Set the parameters t and i, which represent the number of present iteration and gorilla candidate respectively, to be a value of 1.
3- Execute the exploration phase which is repeated with a number equals to the parameter i to choose the best fitness function and best position after i executions of this phase.

4- Execute the exploitation phase which is repeated with a number equals to the parameter i, where the choice of the exploitation mechanism is based on the value of D and W.
5- Increase the parameter t by 1 and repeat steps 3 and 4 for each iteration.
6- Save the best fitness value and best solution per iteration.
7- When the parameter t reaches the maximum number of iterations, the algorithm sequence is stopped, hence the best fitness value and best solution are evaluated from the best ones in all iterations.

In addition, the flowchart of the GTO algorithm is shown in Figure 11 [36], [37]. In the next section, the structure of proposed controller as well as the problem formulation will be presented.

IV. CONTROLLER STRUCTURE AND PROBLEM FORMULATION

The main goal of the proposed controller design is to regulate the frequency response of the hybrid microgrid system when subjected to sudden load disturbances and/or RES fluctuations. The cascaded PI-FOPID controller is proposed in each area to minimize the frequency deviations (ΔF_1, ΔF_2) as well as reducing the tie-line power deviations (ΔP_{tie}). The cascaded control can improve the system performance over single-loop control as the cascaded controller can limit the effect of the disturbances entering the secondary variable on the primary process output. Moreover, it can limit the effect of gain variations on the system performance [45], [46]. In a cascade control arrangement, there are two controllers of which one controller's output drives the set point of another controller. The controller driving the set point is called the primary, outer, or master controller. While the controller receiving the set point is called the secondary, inner or slave controller [47]. Figure 12 shows the block diagram of the cascaded controller structure. The secondary controller in the inner loop can reduce the influence of disturbances $d_1(s)$ on the operation of the control system which takes the set point from the primary controller. Moreover, the inner loop transfer function can be represented in Equation (7) [48], [49]:

$$Y_2(s) = G_2(s)\, U_2(s) \tag{7}$$

where $G_2(s)$ represents the inner process and $U_2(s)$ is the input signal to $G_2(s)$. In addition, the primary controller in the outer loop can regulate the frequency and tie line deviations by minimizing the area control error (ACE). Furthermore, the outer loop transfer function can be represented in Equation (8) [48], [49]:

$$Y(s) = G_1(s)\, U_1(s) + d_1(s) \tag{8}$$

where $G_1(s)$ represents the outer process and $U_1(s)$ is the input signal to $G_1(s)$.

In this study, the FOPID controller is proposed in the inner (or secondary) loop with a transfer function $C_2(s)$.

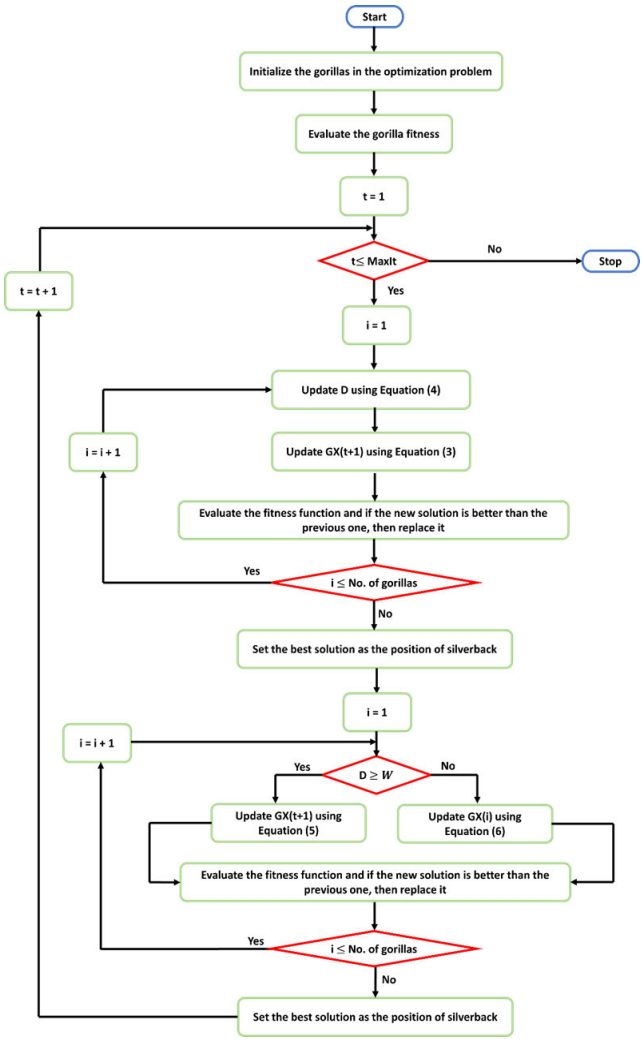

FIGURE 11. Flowchart of the GTO algorithm.

Further, the PI controller is suggested in the outer (or primary) loop with a transfer function $C_1(s)$ to minimize the area control error (ACE) that can be calculated using Equation (7) as follows [2]:

$$ACE_i = B_i \Delta F_i + \Delta P_{tie} \tag{9}$$

The transfer functions of PI and FOPID controllers can be represented using Equations (10) and (11) respectively as follows [31], [49]:

$$C_1(s) = K_{p1} + K_{i1}/s \tag{10}$$

$$C_2(s) = K_{p2} + K_{i2}s^{-\lambda} + K_{d2}s^{\mu} \tag{11}$$

where K_{p1}, K_{i1}, K_{p2}, K_{i2}, K_{d2}, λ and μ are the PI proportional gain, PI integral gain, FOPID proportional gain, FOPID integral gain, FOPID derivative gain, order of integration, and order of derivative, respectively. Figure 13 shows the construction of the cascaded PI-FOPID controller.

The optimal parameters of the PI-FOPID controller will be calculated by minimizing the fitness function (FF) or the

TABLE 3. Comparison between IAE and ITAE results for different SLP in area 2.

Controller	SLP=5%		SLP=10%		SLP=15%		SLP=20%		SLP=25%	
	IAE $\times 10^{-4}$	ITAE $\times 10^{-4}$	IAE $\times 10^{-4}$	ITAE $\times 10^{-4}$	IAE $\times 10^{-4}$	ITAE$\times 1$ 0^{-4}	IAE $\times 10^{-4}$	ITAE $\times 10^{-4}$	IAE $\times 10^{-4}$	ITAE $\times 10^{-4}$
GA-FOPID [27]	1	3.8	2.06	7.68	3.09	11.5	4.13	15	5.3	19
PSO-FOPID [28]	1.04	3.37	2.08	7.42	3.12	11.7	4.17	15.5	5	20
GTO-FOPID	0.99	3.33	1.98	6.66	2.98	11	3.97	13.3	4.9	18
GTO-PI-FOPID	0.00305	0.0109	0.00598	0.0215	0.00914	0.0324	0.013	0.0433	0.016	0.08

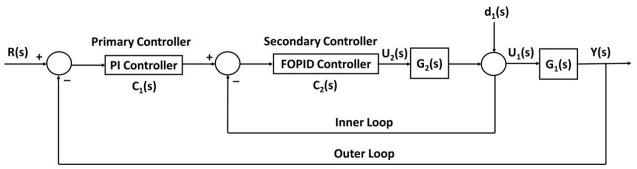

FIGURE 12. Cascaded controller block diagram.

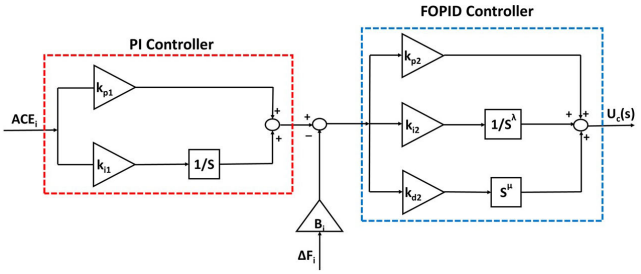

FIGURE 13. The proposed controller structure.

objective function using the GTO algorithm. There are two popular fitness functions used for the LFC design which are the integral absolute error (IAE) and the integral time absolute error (ITAE) [34], [50].

$$IAE = \int_0^{t_s} (|\Delta F_1| + |\Delta F_2| + |\Delta P_{tieline}|)dt \quad (12)$$

$$ITAE = \int_0^{t_s} (|\Delta F_1| + |\Delta F_2| + |\Delta P_{tieline}|)t\,dt \quad (13)$$

where t_s is the time of simulation. The objective function is constrained by the following:

$$\begin{cases} K_{p1,min} \le K_{p1} \le K_{p1,max} \\ K_{i1,min} \le K_{i1} \le K_{i1,max} \\ K_{p2,min} \le K_{p2} \le K_{p2,max} \\ K_{i2,min} \le K_{i2} \le K_{i2,max} \\ K_{d2,min} \le K_{d2} \le K_{d2,max} \\ \lambda_{min} \le \lambda \le \lambda_{max} \\ \mu_{min} \le \mu \le \mu_{max} \end{cases} \quad (14)$$

The lower limits are taken as [0, 0, 0, 0, 0, 0, 0] and the upper limits are [100, 100, 100, 100, 100, 1, 1]. The comparison between the performance results of the proposed controller under both IAE and ITAE fitness functions will be presented in the next section for different scenarios.

V. SIMULATION RESULTS AND DISCUSSION

In this section, the microgrid case study system is tested under numerous scenarios such as different step load perturbations (SLP), random load disturbance, solar irradiance variation, and wind speed fluctuation. In each scenario, the performance of the proposed cascaded PI-FOPID controller tuned by GTO is compared with the single FOPID controller tuned by GA, PSO and GTO. The comparison includes the different fitness function values, namely, IAE and ITAE, as well as the dynamic specifications of ΔF_1, ΔF_2 and ΔP_{tie}.

A. SCENARIO (I): EFFECT OF DIFFERENT STEP LOAD PERTURBATIONS (SLP)

In this scenario, the hybrid microgrid system is tested under 5%, 10%, 15%, and 20% SLP in Area 2. The performance of the GTO based-cascaded PI-FOPID controller is compared with the single GA-FOPID, PSO-FOPID and GTO-FOPID structures. RES fluctuations are not considered in this scenario to study the effect of different SLP only and to investigate the efficiency of the PI-FOPID under different SLP. Each technique procedure is evaluated using 100 iterations, where the number of search agents or population is 30. A convergence curve is shown in Figure 14 to compare the performance of the GTO algorithm with GA, PSO, SHO and MPA algorithms. It can be observed that the GTO algorithm has better convergence than other techniques.

Table 3 shows the optimal fitness function based on IAE and ITAE formulas for different SLP. It can be observed that the proposed GTO-PI-FOPID controller exhibits the lowest (or the best) FF compared to other controllers for 5%, 10%, 15%, 20%, and 25% SLP based on IAE and ITAE objective functions. The proposed GTO-PI-FOPID controller provides the best FF based on IAE that accounts for 0.00305×10^{-4}, 0.00598×10^{-4}, 0.00914×10^{-4}, and 0.013×10^{-4}, 0.016×10^{-4} for 5%, 10%, 15%, 20%, and 25% SLP respectively. Therefore, the IAE objective function is selected for optimizing different controllers, which successfully improves

TABLE 4. Optimal gains based on IAE for different controllers under 5% SLP in area 2.

Controller	Area 1							Area 2						
	K_{p1}	K_{i1}	K_{p2}	K_{i2}	K_{d2}	λ_1	μ_1	K_{p3}	K_{i3}	K_{p4}	K_{i4}	K_{d4}	λ_2	μ_2
GA-FOPID [27]			33.5	26.96	87.56	0.71	0.79			63.05	100	57.45	1	0.48
PSO-FOPID [28]			80.94	35.77	43.47	0.21	0.76			45.09	100	35.38	1	0.49
GTO-FOPID			100	100	100	1	0.009			100	100	100	1	0
GTO-PI-FOPID	100	100	0	100	100	1	1	99.82	100	100	100	100	0.3	0

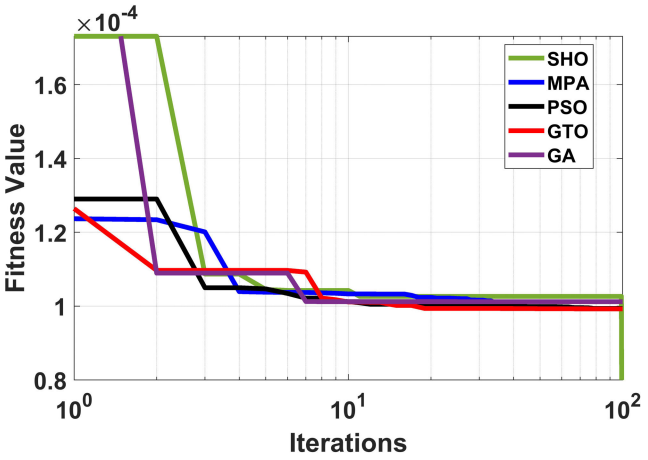

FIGURE 14. Convergence Curve for GA, PSO, SHO, MPA and GTO algorithms.

the dynamic response of the system significantly under different perturbations. Moreover, the optimal gains based on IAE fitness function for different controllers are shown in Table 4 under 5% SLP. Figures 15-19 show the dynamic response of frequency deviations (ΔF_1 and ΔF_2) in each area as well as the tie-line power deviation (ΔP_{tie}) under different SLP. In addition, Tables 5-9 illustrate the transient specifications under 5%, 10%, 15%, 20%, and 25% SLP, respectively using different controllers in terms of the maximum undershoot (MU), maximum overshoot (MO), and settling time (T_s). As shown in Figure 15 (a-c), the proposed GTO-PI-FOPID controller provides the best performance for ΔF_1, ΔF_2 and ΔP_{tie}, however the PSO-FOPID provides the worst performance. Similar to Figure 15, the proposed controller is the best one for 10%, 15%, 20%, and 25% SLP as shown in Figures 16-19, where it is a proof for the robustness and effectiveness of the proposed controller. Further, the MU, MO and T_s are the lowest values using the proposed GTO-PI-FOPID controller as illustrated in Tables 5-9. It can be observed in Table 5 that the proposed controller can improve the MU of ΔF_1 by 99.54%, 99.7%, and 99.74% when compared to GTO-FOPID, GA-FOPID, and PSO-FOPID, respectively. Also, the T_s of ΔF_1 using the GTO-PI-FOPID controller can be improved by 27.27%, 28.5%, and 49.3% as compared to PSO-FOPID, GA-FOPID, and GTO-FOPID, respectively. In addition, the proposed controller can improve the MU of ΔF_2 by 98%, 98.4%, and 98.6% when compared with GA-FOPID, GTO-FOPID, and PSO-FOPID, respectively. Further, the MO of ΔF_2 is enhanced by 98.3%, 99.6%, and 99.8% when compared with GTO-FOPID, GA-FOPID, PSO-FOPID, respectively.

In addition, the T_s of ΔF_2 is further reduced using the proposed controller, which improved by 75.9%, 71% and 50% when compared with GA-FOPID, PSO-FOPID, and GTO-FOPID, respectively. It can be seen that the MO of ΔP_{tie} is decreased using GTO-PI-FOPID, which improved by 99.54%, 99.7%, and 99.74% when compared with GTO-FOPID, GA-FOPID, and PSO-FOPID, respectively. However, the improvement percentage of T_s for ΔP_{tie} is the same as in the case of ΔF_1. The previous improvement percentages of MU, MO, and T_s of ΔF_1, ΔF_2 and ΔP_{tie} in Table 4 are the same in Tables 6-9.

It can be observed that, the GTO algorithm provides the least FF when it is used for tuning the single FOPID and cascaded PI-FOPID controller compared with GA-FOPID and PSO-FOPID. Furthermore, the MU and MO of the system increases as the SLP increases within the acceptable range. However, the T_s with each controller is the same even if the SLP increases.

Moreover, comparisons of the proposed controller with PI, PID, and FOPID controllers are shown in Figure 20. It can be observed that the cascaded PI-FOPID controller is superior to other controllers. However, the PI and PID controller exhibit the same response for ΔF_1, ΔF_2 and ΔP_{tie}.

B. SCENARIO (II): EFFECT OF RANDOM LOAD DISTURBANCE

In this scenario, the performance of the system is studied when it is subjected to a random step load disturbance in

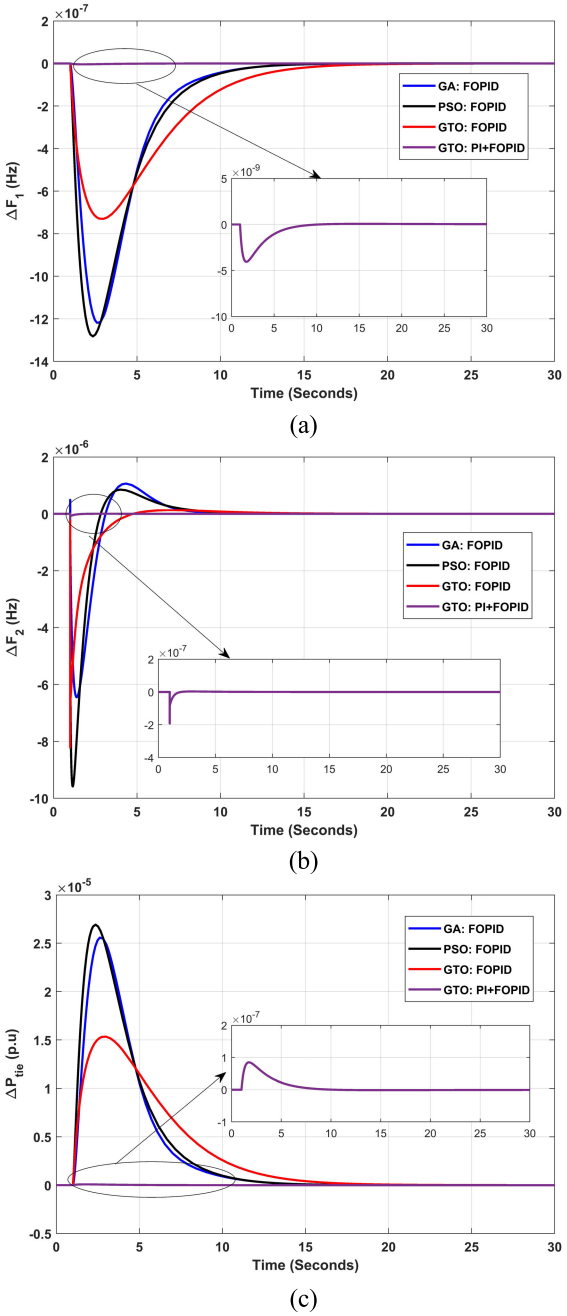

FIGURE 15. Dynamic response under 5% SLP in Area 2: (a) ΔF_1, (b) ΔF_2 and (c) ΔP_{tie}.

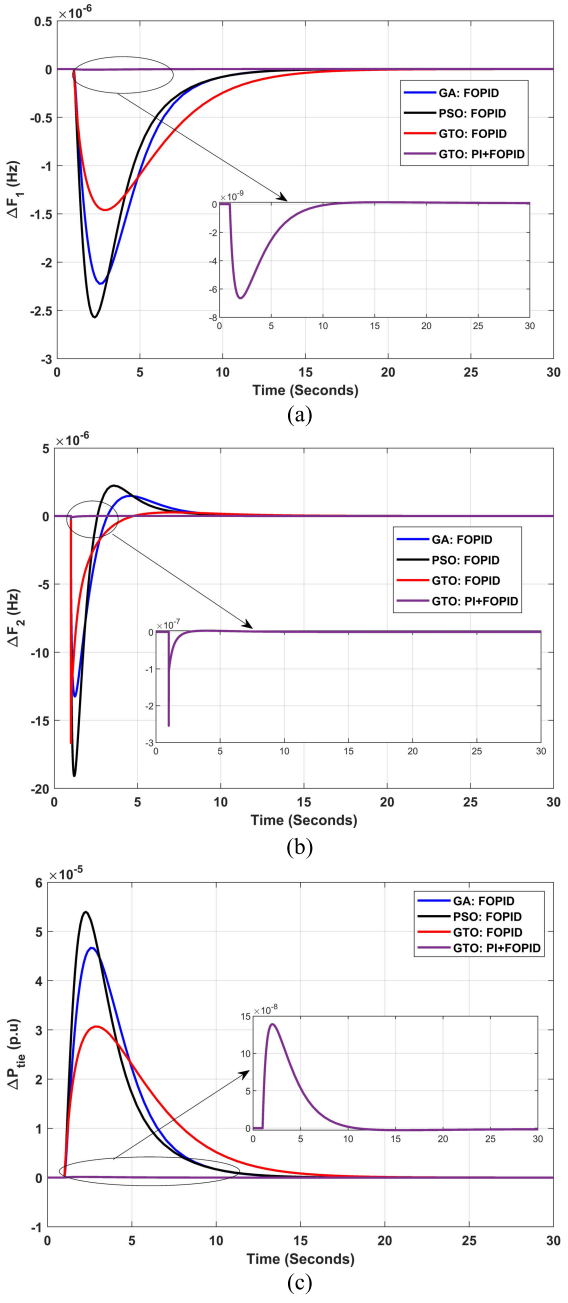

FIGURE 16. Dynamic response under 10% SLP in Area 2: (a) ΔF_1, (b) ΔF_2 and (c) ΔP_{tie}.

Area 2 as shown in Figure 21 to show how different controllers will improve the performance of the system. The load is assumed to vary randomly each 20 seconds and has a limit between 0.06 and 0.135 p.u. Table 10 shows the optimal fitness function based on IAE and ITAE formulas for this scenario. It can be observed that the proposed GTO-PI-FOPID controller exhibits the lowest (or the best) FF compared to other controllers based on IAE and ITAE objective functions. The proposed GTO-PI-FOPID controller provides the best FF based on IAE which is $\mathbf{0.008 \times 10^{-4}}$.

It can be shown that the GTO algorithm has the advantage of providing the lowest FF when it is used for tuning the single FOPID and cascaded PI-FOPID compared to the single FOPID tuned by GA or PSO. As a result, this is further evidence that the GTO algorithm is better than other comparable algorithms as in the previous scenario.

Figure 22 (a-c) shows the dynamic performance of ΔF_1, ΔF_2 and ΔPtie, respectively. The GTO-PI-FOPID controller provides the best transient response when compared to other controllers. For each step load change, the MO, MU and T_s are improved using the cascaded PI-FOPID controller,

TABLE 5. System dynamic results with different controllers under 5% SLP in area 2.

Controller	ΔF_1 (Hz)			ΔF_2 (Hz)			ΔP_{tie} (p.u.)		
	MU (Hz) $\times 10^{-6}$	MO (Hz)	T_s (sec)	MU (Hz) $\times 10^{-6}$	MO (Hz) $\times 10^{-7}$	T_s (sec)	MU (pu)	MO (pu) $\times 10^{-5}$	T_s (sec)
GA-FOPID [27]	-1.1	0	11.2	-6.6	7.3	8.3	0	2.3	11.2
PSO-FOPID [28]	-1.3	0	11	-9.5	11	6.9	0	2.7	11
GTO-FOPID	-0.73	0	15.8	-8.2	1.3	4	0	1.5	15.8
GTO-PI-FOPID	-0.0033	0	8	-0.13	0.022	2	0	0.0069	8

TABLE 6. System dynamic results with different controllers under 10% SLP in area 2.

Controller	ΔF_1 (Hz)			ΔF_2 (Hz)			ΔP_{tie} (p.u.)		
	MU (Hz) $\times 10^{-6}$	MO (Hz)	T_s (sec)	MU (Hz) $\times 10^{-6}$	MO (Hz) $\times 10^{-7}$	T_s (sec)	MU (pu)	MO (pu) $\times 10^{-5}$	T_s (sec)
GA-FOPID [27]	-2.2	0	11.2	-13.2	14.7	8.3	0	4.6	11.2
PSO-FOPID [28]	-2.57	0	11	-19	22.3	6.9	0	5.4	11
GTO-FOPID	-1.46	0	15.8	-16.6	2.64	4	0	3.06	15.8
GTO-PI-FOPID	-0.0066	0	8	-0.25	0.04	2	0	0.013	8

TABLE 7. System dynamic results with different controllers under 15% SLP in area 2.

Controller	ΔF_1 (Hz)			ΔF_2 (Hz)			ΔP_{tie} (p.u.)		
	MU (Hz) $\times 10^{-6}$	MO (Hz)	T_s (sec)	MU (Hz) $\times 10^{-6}$	MO (Hz) $\times 10^{-7}$	T_s (sec)	MU (pu)	MO (pu) $\times 10^{-5}$	T_s (sec)
GA-FOPID [27]	-3.33	0	11.2	-19.8	22	8.3	0	7	11.2
PSO-FOPID [28]	-3.85	0	11	-28.6	33.5	6.9	0	8.09	11
GTO-FOPID	-2.19	0	15.8	-24.8	3.97	4	0	4.6	15.8
GTO-PI-FOPID	-0.0099	0	8	-0.38	0.06	2	0	0.02	8

TABLE 8. System dynamic results with different controllers under 20% SLP in area 2.

Controller	ΔF_1 (Hz)			ΔF_2 (Hz)			ΔP_{tie} (p.u.)		
	MU (Hz) $\times 10^{-6}$	MO (Hz)	T_s (sec)	MU (Hz) $\times 10^{-6}$	MO (Hz) $\times 10^{-7}$	T_s (sec)	MU (pu)	MO (pu) $\times 10^{-5}$	T_s (sec)
GA-FOPID [27]	-4.45	0	11.2	-26.4	29.5	8.3	0	9.3	11.2
PSO-FOPID [28]	-5.14	0	11	-38.1	44.6	6.9	0	10.7	11
GTO-FOPID	-2.92	0	15.8	-33.1	5.3	4	0	6.13	15.8
GTO-PI-FOPID	-0.013	0	8	-0.51	0.083	2	0	0.027	8

TABLE 9. System dynamic results with different controllers under 25% SLP in area 2.

Controller	ΔF_1 (Hz)			ΔF_2 (Hz)			ΔP_{tie} (p.u.)		
	MU (Hz) $\times 10^{-6}$	MO (Hz)	T_s (sec)	MU (Hz) $\times 10^{-6}$	MO (Hz) $\times 10^{-7}$	T_s (sec)	MU (pu)	MO (pu) $\times 10^{-5}$	T_s (sec)
GA-FOPID [27]	-6.9	0	11.2	-33.1	89.5	8.3	0	14.4	11.2
PSO-FOPID [28]	-5.5	0	11	-49.7	22.9	6.9	0	11	11
GTO-FOPID	-3.65	0	15.8	-41.6	6.64	4	0	7.67	15.8
GTO-PI-FOPID	-0.016	0	8	-0.63	0.1	2	0	0.034	8

where the frequency deviations and tie-line power deviation are almost very small compared to other controllers. Additionally, the GTO algorithm provides better dynamic response than GA and PSO algorithms, and therefore the

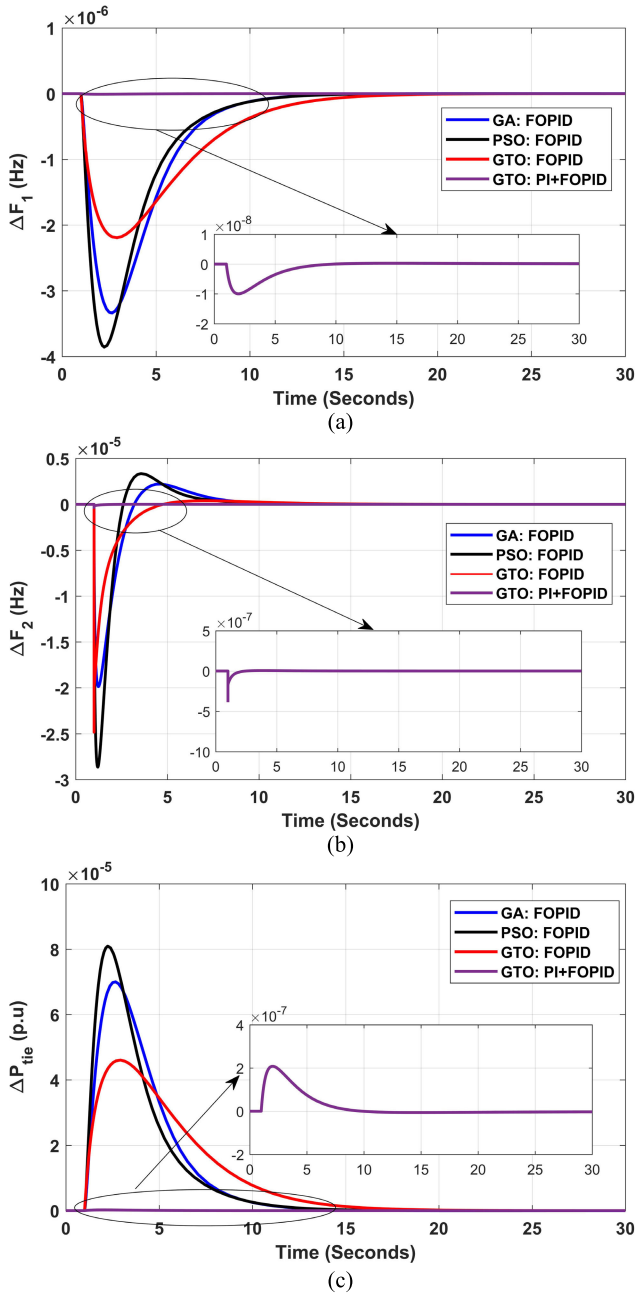

FIGURE 17. Dynamic response under 15% SLP in Area 2: (a) ΔF_1, (b) ΔF_2 and (c) ΔP_{tie}.

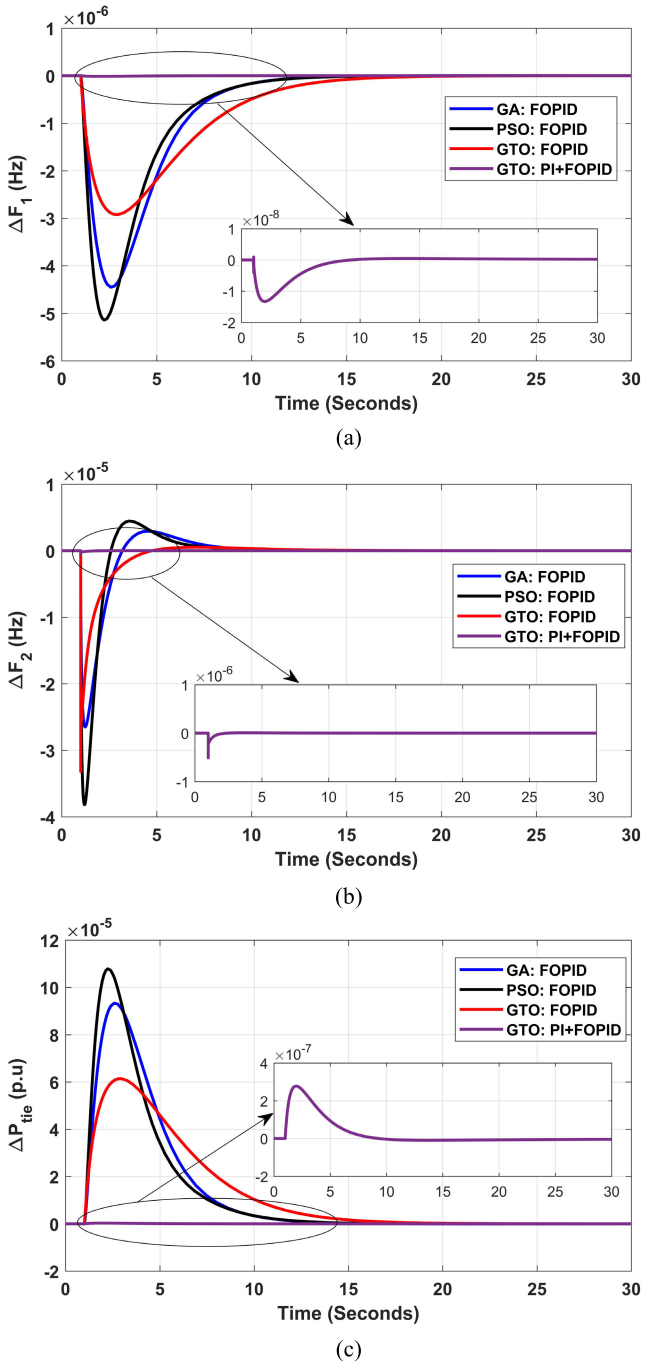

FIGURE 18. Dynamic response under 20% SLP in Area 2: (a) ΔF_1, (b) ΔF_2 and (c) ΔP_{tie}.

TABLE 10. Comparison between IAE and ITAE results for random load disturbance.

Controller	IAE $\times 10^{-4}$	ITAE $\times 10^{-4}$
GA-FOPID [27]	0.0286	4.9
PSO-FOPID [28]	0.0283	5
GTO-FOPID	0.0278	4.7
GTO-PI-FOPID	0.008	0.14

GTO has the efficiency and superiority when the system is exposed to different loads that vary randomly.

C. SCENARIO (III): EFFECT OF RES FLUCTUATIONS

In this scenario, the performance of the system when subjected to variation in solar radiation and wind speed fluctuation is studied. Table 11 shows the optimal fitness function based on IAE and ITAE formulas for this case. It can be observed that the proposed GTO-PI-FOPID controller exhibits the lowest FF compared to other controllers based on IAE and ITAE objective functions. The proposed GTO-PI-FOPID controller provides the best FF based on IAE that

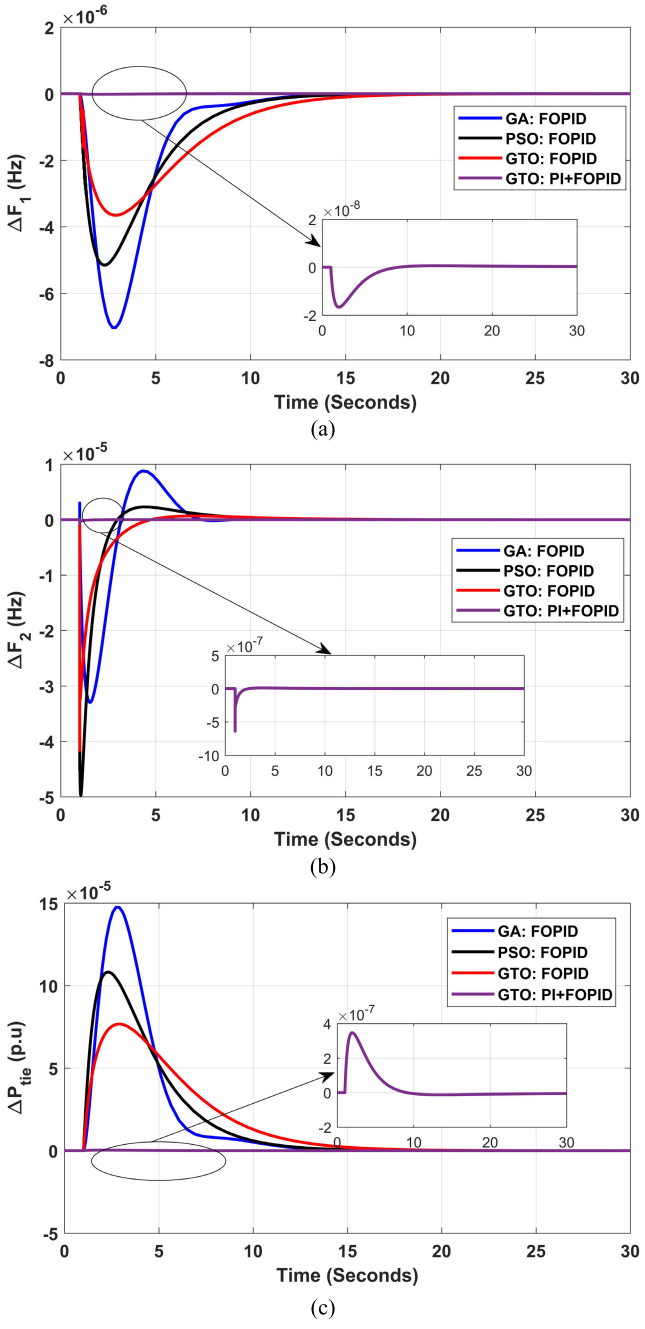

FIGURE 19. Dynamic response under 25% SLP in Area 2: (a) ΔF_1, (b) ΔF_2 and (c) ΔP_{tie}.

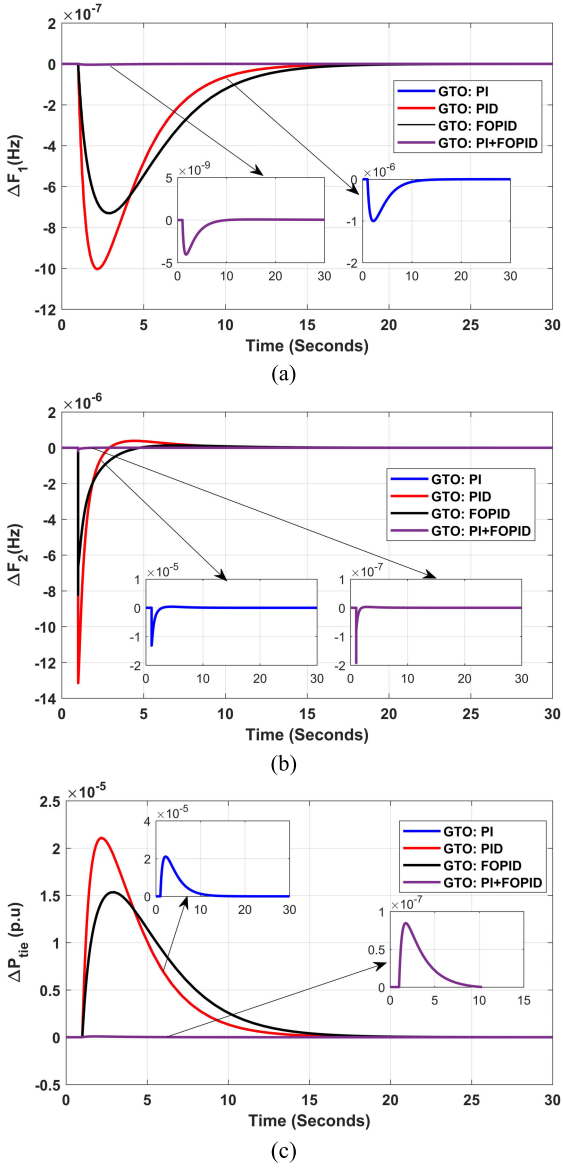

FIGURE 20. Comparison of the proposed algorithm with PI, PID, and FOPID under 5% SLP in Area 2: (a) ΔF_1, (b) ΔF_2 and (c) ΔP_{tie}.

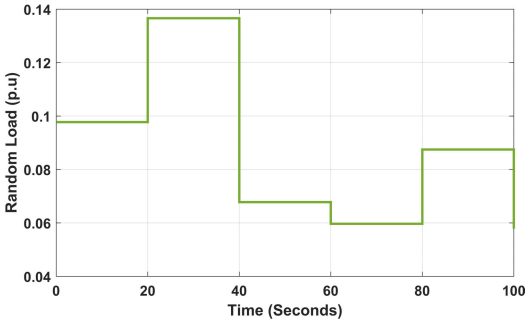

FIGURE 21. Random load profile.

accounts for 0.0209×10^{-4}. In addition, the single FOPID tuned by GTO algorithm provides less FF when it is compared with the single FOPID tuned by GA or PSO. As a result, it is another proof that this algorithm is better than the other compared algorithms like in the previous two scenarios.

Finally, Figure 23 (a-c) represents the dynamic performance of the studied system under RES variations, where the best performance and transient response are achieved by the cascaded PI-FOPID tuned by GTO. In addition, the least fluctuations of ΔF_1, ΔF_2 and ΔP_{tie} can be evaluated by the proposed controller, where they are almost zero when the cascaded controller is compared with the other ones, hence it is zoomed as shown in the mentioned figures. This proves that

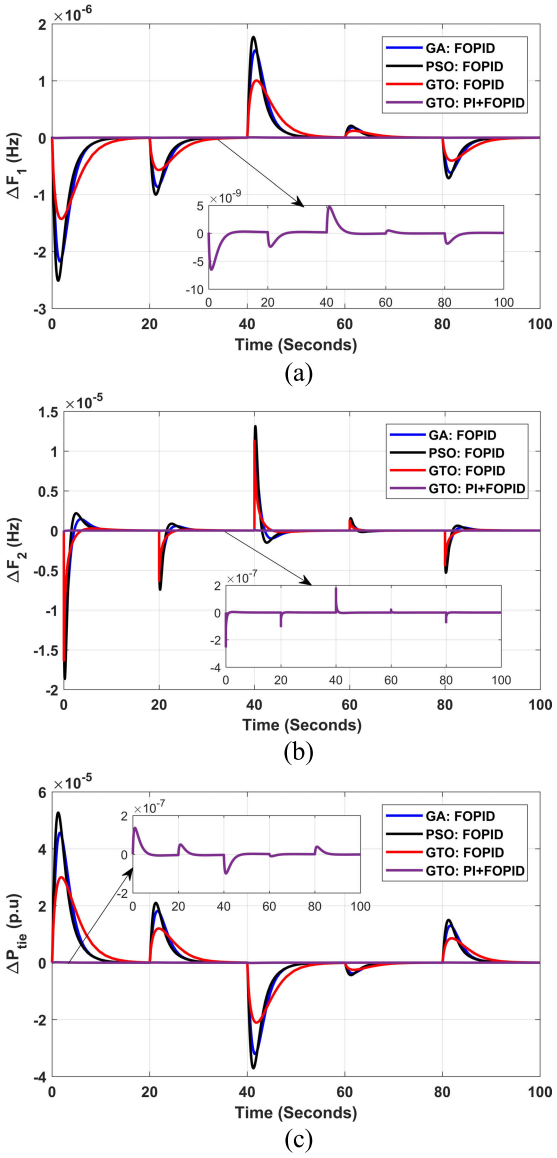

FIGURE 22. Dynamic response under random load disturbance in Area 2: (a) ΔF_1, (b) ΔF_2 and (c) ΔP_{tie}.

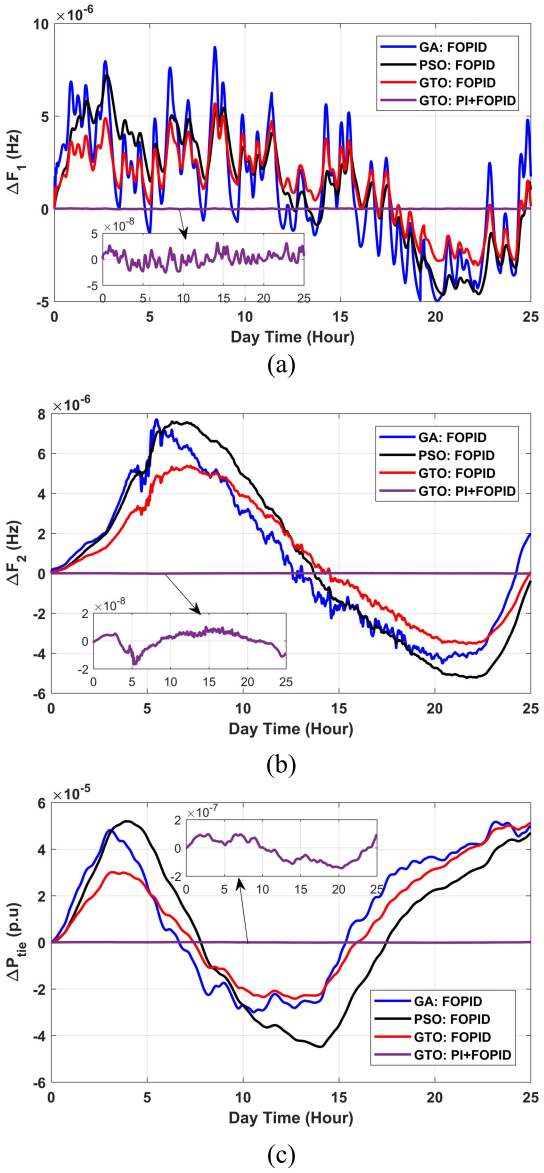

FIGURE 23. Dynamic response under RES fluctuations: (a) ΔF_1, (b) ΔF_2 and (c) ΔP_{tie}.

TABLE 11. Comparison between IAE and ITAE results for RES fluctuations.

Controller	IAE $\times 10^{-4}$	ITAE $\times 10^{-4}$
GA-FOPID [27]	7.9	100
PSO-FOPID [28]	7.6	98
GTO-FOPID	6.6	93
GTO-PI-FOPID	0.0209	0.165

GTO is better than the other algorithm and has more effectiveness when the system is subjected to RES fluctuations.

D. SCENARIO (IV): EFFECT OF SOLAR PV ONLY

This scenario presents the effect of solar irradiance fluctuation only without the wind turbine to study the performance of the system with this disturbance. Figure 24 (a-c) shows that the best performance and transient response are achieved by the proposed controller, where the least fluctuations of ΔF_1, ΔF_2 and ΔP_{tie} can be evaluated in the case of PI-FOPID based GTO algorithm.

E. SCENARIO (V): EFFECT OF WIND TURBINE SYSTEM ONLY

In this scenario, the effect of the wind turbine speed variation is presented only without considering the effect of solar irradiance fluctuation to study the performance of the system with this disturbance. Figure 25 (a-c) shows that the best performance and transient response are achieved by the proposed controller, where the least fluctuations of ΔF_1, ΔF_2 and ΔP_{tie} can be evaluated in the case of PI-FOPID based GTO algorithm.

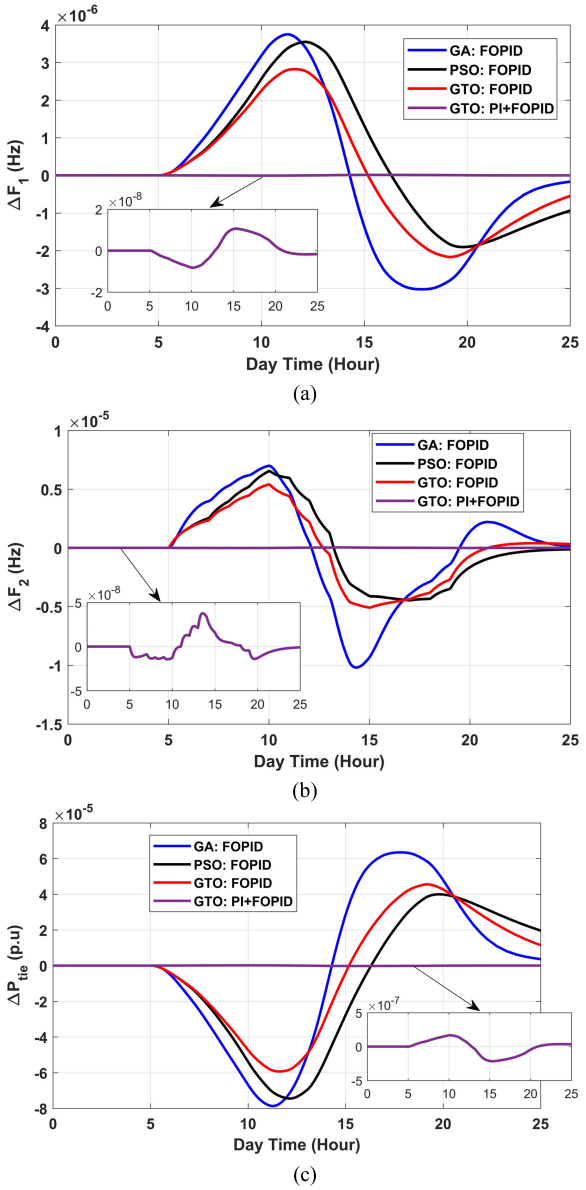

FIGURE 24. Dynamic response under solar PV fluctuations only: (a) ΔF_1, (b) ΔF_2 and (c) ΔP_{tie}.

TABLE 12. Sensitivity analysis for system parameters variation.

System Parameter	Change Percentage	ΔF_1 (Hz)		ΔF_2 (Hz)		ΔP_{tie} (p.u)	
		MU (Hz) $\times 10^{-6}$	MO (Hz)	MU (Hz) $\times 10^{-6}$	MO (Hz) $\times 10^{-7}$	MU (pu)	MO (pu) $\times 10^{-5}$
K_{DE2}	+20%	-0.00313	0	-0.128	0.0209	0	0.00655
	-20%	-0.00354	0	-0.128	0.0238	0	0.0074
K_{BES}	+20%	-0.00292	0	-0.108	0.0196	0	0.0061
	-20%	-0.00387	0	-0.159	0.0259	0	0.00808
K_{tie}	+20%	-0.0038	0	-0.128	0.0225	0	0.00795
	-20%	-0.0028	0	-0.128	0.0217	0	0.00587
B_1	+20%	-0.00283	0	-0.128	0.0239	0	0.0071
	-20%	-0.00403	0	-0.128	0.0202	0	0.00675
B_2	+20%	-0.00283	0	-0.108	0.0107	0	0.00592
	-20%	-0.00403	0	-0.159	0.0312	0	0.00843

F. SCENARIO (VI): SENSITIVITY ANALYSIS TO SYSTEM PARAMETERS VARIATION

In this scenario, the proposed system is subjected to a change in all parameters of the various components to test the

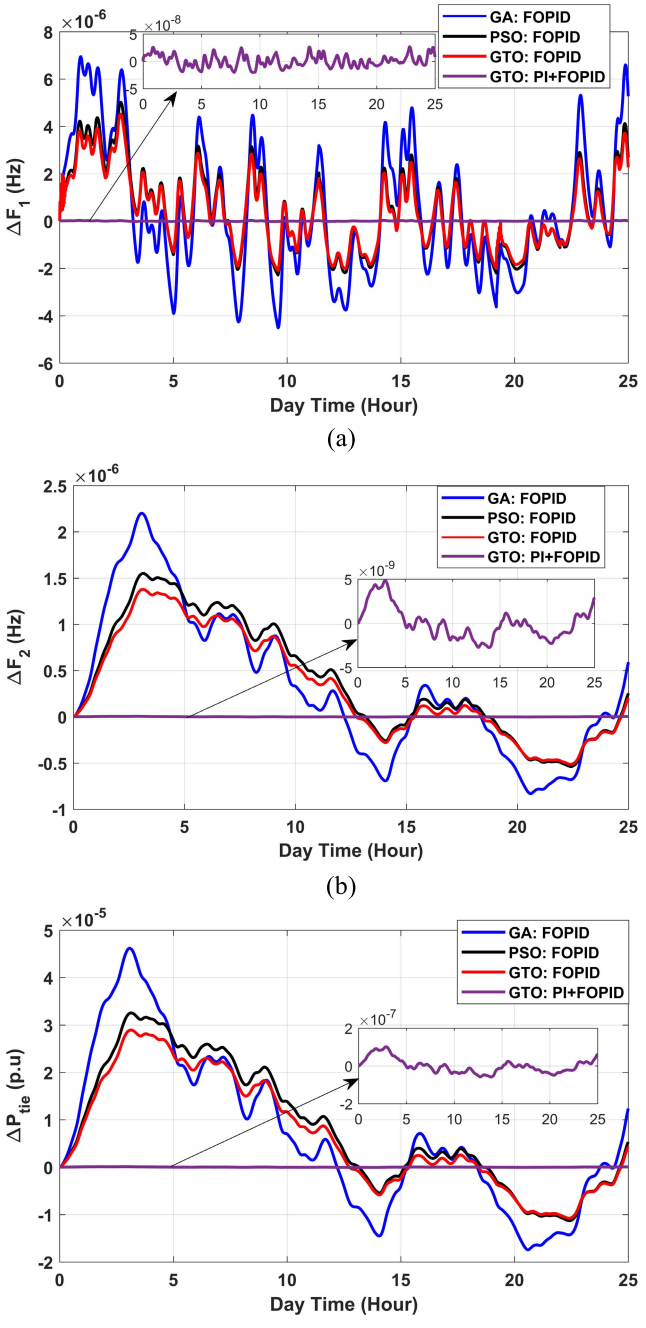

FIGURE 25. Dynamic response under wind turbine system fluctuations only: (a) ΔF_1, (b) ΔF_2 and (c) ΔP_{tie}.

robustness of the cascaded PI-FOPID controller with GTO algorithm. Each parameter of the system components is changed by $\pm$ 20%. However, the dynamic response of the system, which is represented by the MO, MU and T_s, is affected only by changing K_{DE2}, K_{BES}, k_{tie}, B_1 and B_2 are changed. Further, Table 12 shows that the change in MO and MU in both frequency and power deviations is slight and still within the limit, where there is no change in T_s. Hence, this is an indication of the robustness of the proposed

controller which can make the system response unaffected by the change in the system parameters.

VI. CONCLUSION

In this paper, a cascaded PI-FOPID controller has been proposed to enhance the frequency response of a two-area hybrid microgrid system containing photovoltaic, wind turbine generator, diesel engine generator and energy storage systems. The optimal parameters of the proposed controller have been determined using gorilla troops optimizer which is a novel robust optimizer. Moreover, real wind speed data and solar radiation measurements have been used to model the case study system. The performance of the GTO based-cascaded PI-FOPID controller has been compared with the single GA-FOPID, PSO-FOPID and GTO-FOPID structures. Furthermore, three scenarios have been studied and discussed to investigate the effectiveness of the proposed controller in the case of RES fluctuations, random load change and different step load perturbations. The optimization results based on integral absolute error fitness function has provided better dynamic frequency response compared to the integral time absolute error fitness function for all studied cases. The proposed GTO-PI-FOPID controller has improved the fitness function based on integral absolute error that accounts approximately for 0.3% of the best fitness function of the other compared controllers for different SLP respectively. In addition, the proposed cascaded PI-FOPID controller has provided better transient specifications in terms of maximum undershoot, maximum overshoot and settling time for frequency deviations and tie-line power deviation compared to other controllers for all studied scenarios. The results have shown that, the proposed controller has improved the maximum undershoot of the frequency deviation in Area 1 by 99.54%, 99.7%, and 99.74% when compared to GTO-FOPID, GA-FOPID, and PSO-FOPID, respectively. Also, the settling time of the frequency deviation in Area 1 using the GTO-PI-FOPID controller has been improved by 27.27%, 28.5%, and 49.3% as compared to PSO-FOPID, GA-FOPID, and GTO-FOPID, respectively. In addition, the proposed controller has improved the maximum undershoot of the frequency deviation in Area 2 by 98%, 98.4%, and 98.6% when compared to GA-FOPID, GTO-FOPID, and PSO-FOPID, respectively. Further, the maximum overshoot of the frequency deviation in Area 2 has been enhanced by 98.3%, 99.6%, and 99.8% when compared with GTO-FOPID, GA-FOPID, PSO-FOPID, respectively. In addition, the settling time of the frequency deviation in Area 2 has been further reduced using the proposed controller, which improved by 75.9%, 71% and 50% when compared with GA-FOPID, PSO-FOPID, and GTO-FOPID, respectively. The maximum overshoot of the tie-line power deviation has decreased using GTO-PI-FOPID, which has been improved by 99.54%, 99.7%, and 99.74% when compared with GTO-FOPID, GA-FOPID, and PSO-FOPID, respectively. As a result, the cascaded PI-FOPID tuned by the GTO algorithm has shown great superiority and provides excellent dynamic results when applied in the hybrid microgrid system. Furthermore, the proposed controller could be used as a load frequency controller for hybrid microgrid systems which have more than two areas and could achieve the best results when the system is subjected to more different disturbances. For future studies, more practical models can be suggested to model the system components.

REFERENCES

[1] B. Khokhar, S. Dahiya, and K. P. S. Parmar, "A novel hybrid fuzzy PD-TID controller for load frequency control of a standalone microgrid," *Arabian J. Sci. Eng.*, vol. 46, no. 2, pp. 1053–1065, Feb. 2021.

[2] A. H. Yakout, H. Kotb, H. M. Hasanien, and K. M. Aboras, "Optimal fuzzy PIDF load frequency controller for hybrid microgrid system using marine predator algorithm," *IEEE Access*, vol. 9, pp. 54220–54232, 2021.

[3] R. Anaadumba, Q. Liu, B. D. Marah, F. M. Nakoty, X. Liu, and Y. Zhang, "A renewable energy forecasting and control approach to secured edge-level efficiency in a distributed micro-grid," *Cybersecurity*, vol. 4, no. 1, pp. 1–12, Dec. 2021.

[4] M. Kumar and Y. V. Hote, "Maximum sensitivity-constrained coefficient diagram method-based PIDA controller design: Application for load frequency control of an isolated microgrid," *Electr. Eng.*, vol. 103, pp. 2415–2429, Mar. 2021.

[5] M. Ramesh, A. K. Yadav, and P. K. Pathak, "Intelligent adaptive LFC via power flow management of integrated standalone micro-grid system," *ISA Trans.*, vol. 112, pp. 234–250, Jun. 2021.

[6] S. Rajamand, "Load frequency control and dynamic response improvement using energy storage and modeling of uncertainty in renewable distributed generators," *J. Energy Storage*, vol. 37, May 2021, Art. no. 102467.

[7] H. H. Alhelou, M.-E. Hamedani-Golshan, R. Zamani, E. Heydarian-Forushani, and P. Siano, "Challenges and opportunities of load frequency control in conventional, modern and future smart power systems: A comprehensive review," *Energies*, vol. 11, no. 10, p. 2497, 2018.

[8] H. M. Hasanien, "Whale optimisation algorithm for automatic generation control of interconnected modern power systems including renewable energy sources," *IET Gener. Transm. Distrib.*, vol. 12, no. 3, pp. 607–614, 2018.

[9] S. K. Raja, V. P. Badathala, and S. K. Sainadh, "LFC problem by using improved genetic algorithm tuning PID controller," *Int. J. Pure Appl. Math.*, vol. 120, no. 6, pp. 7899–7908, 2018.

[10] R. N. Rao and P. R. K. Reddy, "PSO based tuning of PID controller for a load frequency control in two area power system," *Int. J. Eng. Res. Appl.*, vol. 1, no. 3, pp. 1499–1505, 2015.

[11] B. Saleh, A. M. Yousef, M. Ebeed, F. K. Abo-Elyousr, A. Elnozahy, M. Mohamed, and S. A. M. Abdelwahab, "Design of PID controller with grid connected hybrid renewable energy system using optimization algorithms," *J. Electr. Eng. Technol.*, vol. 16, no. 6, pp. 3219–3233, Nov. 2021, doi: 10.1007/s42835-021-00804-7.

[12] M. A. Sobhy, A. Y. Abdelaziz, H. M. Hasanien, and M. Ezzat, "Marine predators algorithm for load frequency control of modern interconnected power systems including renewable energy sources and energy storage units," *Ain Shams Eng. J.*, Jun. 2021, doi: 10.1016/j.asej.2021.04.031.

[13] A. A. El-Fergany and M. A. El-Hameed, "Efficient frequency controllers for autonomous two-area hybrid microgrid system using social-spider optimiser," *IET Gener., Transmiss. Distrib.*, vol. 11, no. 3, pp. 637–648, Feb. 2017.

[14] P. Mehta, P. Bhatt, and V. Pandya, "Optimized coordinated control of frequency and voltage for distributed generating system using cuckoo search algorithm," *Ain Shams Eng. J.*, vol. 9, no. 4, pp. 1855–1864, Dec. 2018.

[15] A. K. Barik and D. C. Das, "Integrated resource planning in sustainable energy-based distributed microgrids," *Sustain. Energy Technol. Assessments*, vol. 48, Dec. 2021, Art. no. 101622.

[16] M. Khamies, G. Magdy, M. E. Hussein, F. A. Banakhr, and S. Kamel, "An efficient control strategy for enhancing frequency stability of multi-area power system considering high wind energy penetration," *IEEE Access*, vol. 8, pp. 140062–140078, 2020.

[17] M. Khamies, G. Magdy, M. Ebeed, and S. Kamel, "A robust PID controller based on linear quadratic Gaussian approach for improving frequency stability of power systems considering renewables," *ISA Trans.*, vol. 117, pp. 118–138, Nov. 2021.

[18] Y. Mi, X. He, X. Hao, Z. Li, Y. Fu, C. Wang, and J. Wang, "Frequency control strategy of multi-area hybrid power system based on frequency division and sliding mode algorithm," *IET Gener., Transmiss. Distrib.*, vol. 13, no. 7, pp. 1145–1152, Apr. 2019.

[19] G. Magdy, G. Shabib, A. A. Elbaset, and Y. Mitani, "Frequency stabilization of renewable power systems based on MPC with application to the Egyptian grid," *IFAC-PapersOnLine*, vol. 51, no. 28, pp. 280–285, 2018.

[20] C. Zhang, S. Wang, and Q. Zhao, "Distributed economic MPC for LFC of multi-area power system with wind power plants in power market environment," *Int. J. Electr. Power Energy Syst.*, vol. 126, Mar. 2021, Art. no. 106548.

[21] M. Gheisarnejad, "An effective hybrid harmony search and cuckoo optimization algorithm based fuzzy PID controller for load frequency control," *Appl. Soft Comput.*, vol. 65, pp. 121–138, Apr. 2018.

[22] D. Tripathy, N. B. D. Choudhury, and B. K. Sahu, "Grasshopper optimization algorithm-based fuzzy-2DOF-PID controller for LFC of interconnected system with nonlinearities," *Int. J. Social Ecol. Sustain. Develop.*, vol. 12, no. 3, pp. 11–29, Jul. 2021.

[23] A. Latif, S. M. S. Hussain, D. C. Das, T. S. Ustun, and A. Iqbal, "A review on fractional order (FO) controllers' optimization for load frequency stabilization in power networks," *Energy Rep.*, vol. 7, pp. 4009–4021, Nov. 2021.

[24] M. Shouran, F. Anayi, M. Packianather, and M. Habil, "Load frequency control based on the Bees algorithm for the great Britain power system," *Designs*, vol. 5, no. 3, p. 50, Aug. 2021.

[25] R. Ramachandran, J. S. Kumar, B. Madasamy, and V. Veerasamy, "A hybrid MFO-HNN tuned self-adaptive FOPID controller for ALFC of renewable energy integrated hybrid power system," *IET Renew. Power Gener.*, vol. 15, no. 7, pp. 1582–1595, May 2021.

[26] F. Babaei, Z. B. Lashkari, A. Safari, M. Farrokhifar, and J. Salehi, "Salp swarm algorithm-based fractional-order PID controller for LFC systems in the presence of delayed EV aggregators," *IET Electr. Syst. Transp.*, vol. 10, no. 3, pp. 259–267, Sep. 2020.

[27] N. Bayati, A. Dadkhah, B. Vahidi, and S. H. H. Sadeghi, "Fopid design for load-frequency control using genetic algorithm," *Sci. Int.*, vol. 27, no. 4, pp. 3089–3094, 2015.

[28] I. Pan and S. Das, "Fractional order AGC for distributed energy resources using robust optimization," *IEEE Trans. Smart Grid*, vol. 7, no. 5, pp. 2175–2186, Sep. 2016.

[29] A. Tabak, "Fractional order frequency proportional-integral-derivative control of microgrid consisting of renewable energy sources based on multi-objective grasshopper optimization algorithm," *Trans. Inst. Meas. Control*, vol. 9, Aug. 2021, Art. no. 01423312211034660.

[30] I. Pan and S. Das, "Frequency domain design of fractional order PID controller for AVR system using chaotic multi-objective optimization," 2013, *arXiv:1306.3682*.

[31] E. A. Mohamed, E. M. Ahmed, A. Elmelegi, M. Aly, O. Elbaksawi, and A.-A. A. Mohamed, "An optimized hybrid fractional order controller for frequency regulation in multi-area power systems," *IEEE Access*, vol. 8, pp. 213899–213915, 2020.

[32] A. Latif, D. C. Das, A. K. Barik, and S. Ranjan, "Illustration of demand response supported co-ordinated system performance evaluation of YSGA optimized dual stage PIFOD-(1 + PI) controller employed with wind-tidal-biodiesel based independent two-area interconnected microgrid system," *IET Renew. Power Gener.*, vol. 14, no. 6, pp. 1074–1086, Apr. 2020.

[33] H. H. Fayek and P. Kotsampopoulos, "Central tunicate swarm NFOPID-based load frequency control of the Egyptian power system considering new uncontrolled wind and photovoltaic farms," *Energies*, vol. 14, no. 12, p. 3604, Jun. 2021.

[34] E. Çelik, "Design of new fractional order PI–fractional order PD cascade controller through dragonfly search algorithm for advanced load frequency control of power systems," *Soft Comput.*, vol. 25, no. 2, pp. 1193–1217, Jan. 2021.

[35] E. M. Ahmed, A. Elmelegi, A. Shawky, M. Aly, W. Alhosaini, and E. A. Mohamed, "Frequency regulation of electric vehicle-penetrated power system using MPA-tuned new combined fractional order controllers," *IEEE Access*, vol. 9, pp. 107548–107565, 2021.

[36] B. Abdollahzadeh, F. Soleimanian Gharehchopogh, and S. Mirjalili, "Artificial gorilla troops optimizer: A new nature-inspired metaheuristic algorithm for global optimization problems," *Int. J. Intell. Syst.*, vol. 36, no. 10, pp. 5887–5958, Oct. 2021.

[37] A. Ginidi, S. M. Ghoneim, A. Elsayed, R. El-Sehiemy, A. Shaheen, and A. El-Fergany, "Gorilla troops optimizer for electrically based single and double-diode models of solar photovoltaic systems," *Sustainability*, vol. 13, no. 16, p. 9459, Aug. 2021.

[38] S. Patel, B. Mohanty, and H. M. Hasanien, "Competition over resources optimized fuzzy TIDF controller for frequency stabilization of hybrid micro-grid system," *Int. Trans. Electr. Energy Syst.*, vol. 30, no. 9, 2020, Art. no. e12513.

[39] Vigya, T. Mahto, H. Malik, V. Mukherjee, M. A. Alotaibi, and A. Almutairi, "Renewable generation based hybrid power system control using fractional order-fuzzy controller," *Energy Rep.*, vol. 7, pp. 641–653, Nov. 2021.

[40] A. Bakeer, G. Magdy, A. Chub, and H. Bevrani, "A sophisticated modeling approach for photovoltaic systems in load frequency control," *Int. J. Electr. Power Energy Syst.*, vol. 134, Jan. 2022, Art. no. 107330.

[41] I. I. EL-sharkawy, H. Abdelmaguid, B. B. Saha, S. Koyama, and T. Miyazaki, "Performance investigation of a solar-powered adsorption cooling system: A case study for Egypt," in *Proc. Int. Symp. Innov. Mater. Processes Energy Syst. (IMPRES)*, Fukuoka, Japan, 2013, pp. 1–7.

[42] C.-M. Huang, Y.-C. Huang, S.-J. Chen, and S.-P. Yang, "A hierarchical optimization method for parameter estimation of diesel generators," *IEEE Access*, vol. 8, pp. 176467–176479, 2020.

[43] J. Yang, Z. Zeng, Y. Tang, J. Yan, H. He, and Y. Wu, "Load frequency control in isolated micro-grids with electrical vehicles based on multivariable generalized predictive theory," *Energies*, vol. 8, no. 3, pp. 2145–2164, Mar. 2015.

[44] F. Amiri and M. Moradi, "Coordinated control of LFC and SMES in the power system using a new robust controller," *Iranian J. Electr. Electron. Eng.*, vol. 17, no. 4, p. 1912, 2021.

[45] Y. Arya, N. Kumar, P. Dahiya, G. Sharma, E. Çelik, S. Dhundhara, and M. Sharma, "Cascade-IλSμN controller design for AGC of thermal and hydro-thermal power systems integrated with renewable energy sources," *IET Renew. Power Gener.*, vol. 15, no. 3, pp. 504–520, Feb. 2021.

[46] A. H. Yakout, M. A. Attia, and H. Kotb, "Marine predator algorithm based cascaded PIDA load frequency controller for electric power systems with wave energy conversion systems," *Alexandria Eng. J.*, vol. 60, no. 4, pp. 4213–4222, Aug. 2021.

[47] V. Veerasamy, N. I. A. Wahab, R. Ramachandran, M. L. Othman, H. Hizam, A. X. R. Irudayaraj, J. M. Guerrero, and J. S. Kumar, "A Hankel matrix based reduced order model for stability analysis of hybrid power system using PSO-GSA optimized cascade PI-PD controller for automatic load frequency control," *IEEE Access*, vol. 8, pp. 71422–71446, 2020.

[48] D. Guha, P. K. Roy, and S. Banerjee, "Equilibrium optimizer-tuned cascade fractional-order 3DOF-PID controller in load frequency control of power system having renewable energy resource integrated," *Int. Trans. Electr. Energy Syst.*, vol. 31, no. 1, Jan. 2021, Art. no. e12702, doi: 10.1002/2050-7038.12702.

[49] A. A. A. El-Ela, R. A. El-Sehiemy, A. M. Shaheen, and A. E.-G. Diab, "Enhanced coyote optimizer-based cascaded load frequency controllers in multi-area power systems with renewable," *Neural Comput. Appl.*, vol. 33, no. 14, pp. 8459–8477, Jan. 2021.

[50] Y. Arya, "A new optimized fuzzy FOPI-FOPD controller for automatic generation control of electric power systems," *J. Franklin Inst.*, vol. 356, no. 11, pp. 5611–5629, Jul. 2019.

MOETASEM ALI received the B.Sc. degree in electrical engineering from the Faculty of Engineering, Alexandria University, Alexandria, Egypt, in 2018. He is currently a Teaching Assistant with the Electrical Department, Faculty of Engineering, Alexandria University. His current research interests include power system analysis, smart grids, power systems control, and renewable energy sources.

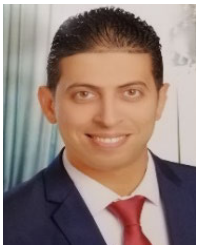

HOSSAM KOTB received the B.Sc., M.Sc., and Ph.D. degrees in electrical engineering from the Faculty of Engineering, Alexandria University, Alexandria, Egypt, in 2009, 2013, and 2020, respectively. His Ph.D. research work is focused on the performance enhancement of renewable energy conversion systems. He is currently an Assistant Professor with the Department of Electrical Power and Machines, Faculty of Engineering, Alexandria University. His research interests include power system analysis, electrical drives, modern control techniques, smart grids, and renewable energy systems. He is a reviewer for many international journals.

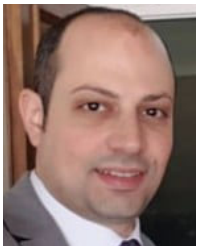

KAREEM M. ABORAS received the B.Sc., M.Sc., and Ph.D. degrees in electrical engineering from the Faculty of Engineering, Alexandria University, Alexandria, Egypt, in 2010, 2015, and 2020, respectively. His Ph.D. research work is focused on the performance enhancement of renewable energy conversion systems. He is currently an Assistant Professor with the Department of Electrical Power and Machines, Faculty of Engineering, Alexandria University. His research interests include power electronics, control, drives, power systems, and renewable energy systems. He is a reviewer of IET journal.

NABIL H. ABBASY (Senior Member, IEEE) received the B.Sc. and M.Sc. degrees (Hons.) in electrical engineering from Alexandria University, Egypt, and the Ph.D. degree from IIT, Chicago, IL,USA, in 1988. He worked at Clarkson University, NY, USA, and PAAET, Kuwait. He is currently an Emeritus Professor at Alexandria University. He has authored and coauthored more than 90 conference papers and journal articles. His research interests include monitoring and protection of microgrids, smart grids, and modern energy management systems. He served as an Ex-Chairman for the Department of Electrical Engineering and the Executive Manager of the Specialized Scientific Programs at AU. He is an Editor of IEEE TRANSACTIONS ON SMART GRID and an Associate Editor of *MPCE Journal*.